Strategies for enzymological studies and measurements of biological molecules with the cytolysin A nanopore

Wloka, Carsten; Galenkamp, Nicole S; van der Heide, Nieck J; Lucas, Florian L R; Maglia, Giovanni

Published in:
Methods in Enzymology

DOI:
10.1016/bs.mie.2021.01.007

Publication date:
2021

CHAPTER NINETEEN

Strategies for enzymological studies and measurements of biological molecules with the cytolysin A nanopore

Carsten Wloka*, Nicole S. Galenkamp, Nieck J. van der Heide, Florian L.R. Lucas, and Giovanni Maglia*

Groningen Biomolecular Sciences & Biotechnology Institute, University of Groningen, Groningen, The Netherlands

*Corresponding authors: e-mail address: c.wloka@rug.nl; g.maglia@rug.nl

Contents

Abstract

Pore-forming toxins are used in a variety of biotechnological applications. Typically, individual membrane proteins are reconstituted in artificial lipid bilayers where they form water-filled nanoscale apertures (nanopores). When a voltage is applied, the ionic current passing through a nanopore can be used for example to sequence biopolymers, identify molecules, or to study chemical or enzymatic reactions at the single-molecule level. Here we present strategies for studying individual enzymes and measuring molecules, also in highly complex biological samples such as blood.

Methods in Enzymology, Volume 649
ISSN 0076-6879
https://doi.org/10.1016/bs.mie.2021.01.007

1. Introduction: The ClyA nanopore

The transmembrane protein cytolysin A (ClyA) is a pore-forming toxin, which is secreted by several bacteria (Ludwig, Bauer, Benz, Bergmann, & Goebel, 1999; von Rhein et al., 2009). We and others use ClyA originating from *Salmonella typhi* (Kwak, Kim, Lee, Ryu, & Chi, 2020; Soskine, Biesemans, De Maeyer, & Maglia, 2013; Soskine et al., 2012; Soskine, Biesemans, & Maglia, 2015; Wloka et al., 2017) but notice that the ortholog of *Escherichia coli* ClyA can yield similar results (Li, Lee, Shorkey, Chen, & Chen, 2020). A ClyA pore consists of multiple identical subunits of 34 kDa. X-ray and cryo-EM structures revealed that these monomeric pore-forming subunits can assemble into different quaternary structures consisting of 12, dodecamer, (Mueller, Grauschopf, Maier, Glockshuber, & Ban, 2009; Peng, de Souza Santos, Li, Tomchick, & Orth, 2019) (Fig. 1A and B), 13, tridecamer, (Eifler et al., 2006; Peng et al., 2019) or 14 subunits, tetradecamer, (Peng et al., 2019). In lipid bilayer experiments we also observe three different nanopore species as we discuss later, which we refer to as type I pore, likely the dodecamer, (Soskine et al., 2012), type II pore, likely the tridecamer, (Soskine et al., 2013) and type III pore, likely the tetradecamer, (Soskine et al., 2013). Type III ClyA has a lifetime of only few minutes in lipid bilayers, while type I and type II nanopores can be used for h in electrical recordings. Type I ClyA (Fig. 1A and B) can accommodate proteins of about 20–45 kDa (as monomers), and it has been the main nanopore used in our laboratory.

Currently we mainly use a ClyA variant we call ClyA-AS. ClyA-AS is built upon a cysteine-free variant of *S. typhi* ClyA, replacing two native cysteine residues. Further mutations were introduced, *via* directed evolution, to increase the soluble expression of the monomer and to enhance stability of the nanopore in electrophysiological experiments with a more homogeneous nanopore conductance (Soskine et al., 2013). ClyA-AS (containing a 5-histidine tag at the C-terminus) differs from the *S. typhi* wildtype sequence ultimately in the following positions: C87A, L99Q, E103G, F166Y, I203V, C285S, K294R and H307Y. The ClyA-AS type I pore has a total length of 14 nm. The lumen of the pore consists of two compartments: the 10 nm long *cis* lumen with a 6 nm internal diameter and a 4 nm long *trans* constriction with a 3 nm internal diameter (Fig. 1) (Soskine et al., 2013).

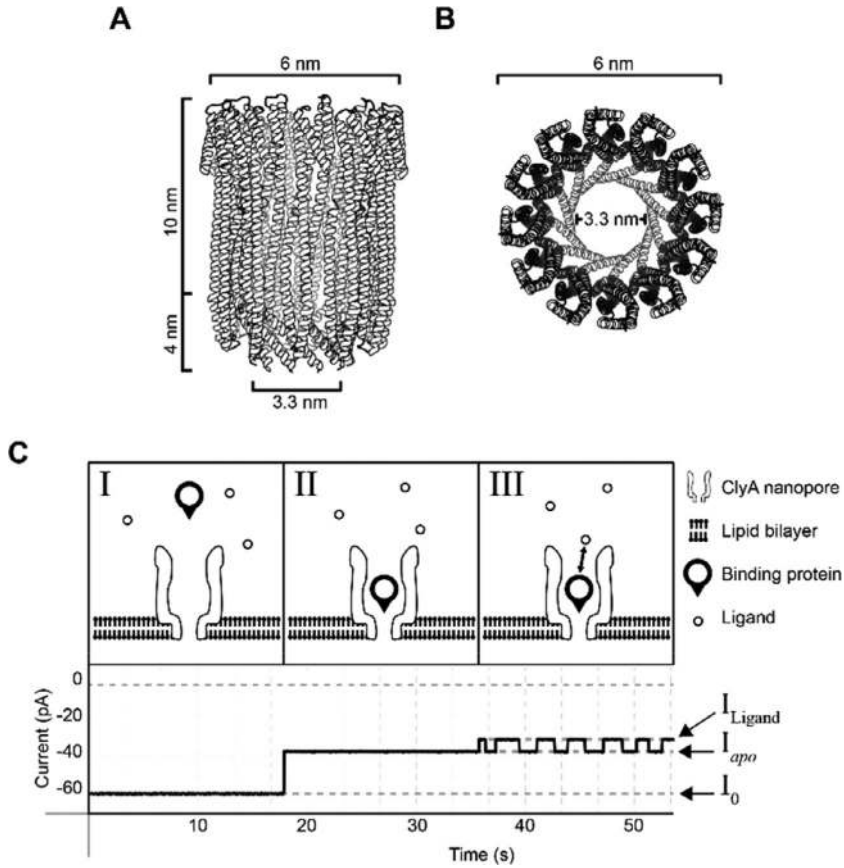

Fig. 1 Crystal structure of cytolysin A (ClyA) and schematic of the basic principle of nanopore enzymology. (A and B) Crystal structure of *E. coli* ClyA (PDB: 6MRT) with side view (A) and top view (B). (C) (I) Drawing of protein capture inside ClyA with (II) a protein captured inside ClyA and (III) ligand binding to the protein confined within ClyA.

The ClyA-AS pore has a negatively charged interior and displays cation-selectivity (Ludwig et al., 1999; von Rhein et al., 2009) in solutions containing up to about 2 M NaCl (Willems et al., 2020). When an external bias is applied, a significant electroosmotic flow (EOF) is generated that allows the trapping of proteins inside the nanopore, typically for seconds to minutes. Although in this method we focus on protein enzymology and quantitative detection of small molecules, we would like to point out that ClyA could also be used for studies of nucleic acids. We developed two variants, ClyA-R and ClyA-RR, in which one or two rings of

positively charged arginine residues have been introduced. These positive charges allow for the translocation of, for example, double-stranded and single-stranded DNA at near-physiological salt concentrations (150 mM NaCl, 15 mM Tris–HCl, pH 7.5) (Franceschini, Brouns, Willems, Carlon, & Maglia, 2016; Nomidis, Hooyberghs, Maglia, & Carlon, 2018).

2. The experimental setup

For general technical instructions about the electrophysiological setup, we would like to refer to a previous publication (Maglia, Heron, Stoddart, Japrung, & Bayley, 2010). The methods presented here describe our experience with the ClyA nanopore for the purposes of enzymological studies and quantitative detection of small molecules. For small molecule detection, we rely on protein adaptors trapped inside the ClyA nanopore whose signal elicited in the pore changes upon binding of their cognate ligand. For most of our experiments we commonly use a near-physiological buffer to create a near-native environment for protein studies. This is in contrast with smaller nanopores such as the αHL or MspA nanopores, which are usually sampled at higher ionic strengths (typically 1 M NaCl or KCl). However, since ClyA is a comparably larger pore it allows a large current flow, even at low ionic strength. This represents a key advantage when working with most proteins. If needed, however, ClyA is also stable in various other conditions, including very high (3 M) salt concentrations and different acidity. However, ionic strengths higher than 0.5 M reduce the EOF across the nanopore (Willems et al., 2020), and usually alter dwell times of proteins inside the nanopore.

The detailed protocol for the expression and purification of ClyA nanopores was described recently (Galenkamp et al., 2021). Briefly, we purify ClyA monomers using standard his-tag purification and dilute the protein concentration to 1 mg/mL. Oligomerization is triggered by addition of 0.2% DDM (*n*-dodecyl β-D-maltoside) to the solution of monomers and subsequent incubation for 30 min at 37 °C. After oligomerization, blue native PAGE sample buffer is added to the solution. The different oligomeric forms of the ClyA pores are then separated on a blue native PAGE gel using precast gels (4–20% gel, Criterion Cell system, BioRad). To prepare the pre-cast gels, the buffer chamber and the top compartment of the gel is filled with 1 × native running buffer (Novex). Per well we load 45 μL of the ClyA mixture. The gel is then run for 10 min at 120 V with 2 mL of 20 × cathode buffer additive added to the top compartment of the gel

already containing 1 × native running buffer and mixed by pipetting. The cathode buffer additive prevents membrane proteins from aggregating during separation and removes detergents. After 10 min, the cathode buffer additive is replaced with fresh 1 × native running buffer and continues to run for another 60 min at 120 V. The blue-stained protein bands are cut out of the gel with a surgical blade. The acquired gel bands are further cut into even smaller pieces and stored at −80 °C. When needed, the ClyA oligomers are extracted by submerging a gel piece in 20–50 μL of the respective recording buffer supplemented with 0.2% DDM and 1 mM EDTA. The extracted ClyA oligomers can be stored at 4 °C for several weeks. The extracted ClyA oligomers are not stable when they are subsequently frozen. Therefore, long-term storage requires the oligomers to be stored and frozen while embedded within native gel bands.

3. How to obtain a single channel

We prepare planar lipid bilayers consisting of 1,2-diphytanoyl-*sn*-glycero-3-phosphocholine (DPhPC) using the Montal-Mueller method (Maglia et al., 2010; Montal & Mueller, 1972) in an open vertical lipid bilayer device (referred to as the chamber) as described previously (Maglia et al., 2010). It is important to note that the likelihood of ClyA insertion into the lipid bilayer is largely dependent on the surface area of the lipid bilayer. Since the lipid bilayer acts as a capacitor, the surface area can be estimated by determining the observed capacitance. How the capacitance of a lipid bilayer can be estimated was shown previously (Maglia et al., 2010). To summarize, and extend, we utilize the current-voltage relation for capacitors, $I(t) = C \times dV(t)dt^{-1}$. Since we apply a constant voltage ramp of $1\,V\,s^{-1}$ (Maglia et al., 2010), the current measured in Amperes corresponds to the capacitance of the bilayer in Farads. Typically, we apply a voltage ramp between +15 and −15 mV over a period of 30 ms to create a triangular wave profile with a constant voltage ramp of +1 or $-1\,V\,s^{-1}$. The resulting current appears as a square wave, due to the constant switching between positive and negative voltage ramps, where the current amplitude is equal to the capacitance. Subsequently, the capacitance is directly proportional to the surface area and thickness of the lipid membrane, a dielectric material, following the equation for the capacitance of a dielectric, $C = \varepsilon \times A \times d^{-1}$, where C is the capacitance in Farad, ε is the absolute permittivity, A is the area of the bilayer in square meter and d its thickness in meter. While it is difficult to give a well-determined absolute permittivity

of the bilayer (Nymeyer & Zhou, 2008), this relationship is still useful to estimate the size of our bilayer and to establish if we formed bi- or multilayered lipid membranes. In practice, the first time that an electrophysiology chamber is used, multiple bilayers are formed and broken while the resulting capacitance of the lipid bilayers is carefully noted. Typical bilayers in an aperture with a diameter of approximately 100 µm exhibit a capacitance, according to the equations above, of 60 to 200 pF and allow the reconstitution of ClyA-AS. In our experience, we observe that ClyA insertion is especially efficient in bilayers with an observed capacitance of 80 to 150 pF equal to a measured current of 80 to 150 pA. While it is possible to use larger than 150 pF bilayers, this results in an increase in noise due to the simultaneous increase in capacitance of the bilayer. Larger bilayers display more noise while smaller bilayers make it difficult to obtain pores. Because bilayers can get smaller over time (shrink), the size of the bilayer should be checked regularly during experiments.

To obtain single nanopores, we commonly use a small pipette tip (without an attached pipette) to briefly touch the extraction buffer containing the nanopores. The tip is then subsequently immerged in the *cis* compartment. If nanopore insertions cannot be observed, larger volumes of stock nanopore solution are added to the electrophysiology chamber. For every new addition we take a fresh pipette tip. If, after addition of pores, a bilayer cannot be formed anymore with ease, it is likely that too many pores were added. Because there is no DDM in our recording buffer, pore insertion becomes more difficult over time (i.e. the pores are likely to fall apart), so it can be advisable to simply wait a couple of minutes before trying to form a bilayer again. Also, it is possible to add an extra dilution step before the addition of pores. This can be done, for example, by swirling the pipette tip in a separate tube of recording buffer before adding it to the *cis* chamber. This step removes excess pores on the tip. We cannot calculate a precise concentration, due to the very low amount of nanopores added, but we estimate sub-nanomolar pore concentrations.

For pore insertion, we routinely apply −35 mV in a "Gap Free" protocol (Clampfit 10.7), a protocol for continuous observation of current (Maglia et al., 2010), and wait for a stepwise current increase, signifying pore insertion. It can be advisable to expose the bilayer to alternating voltages of ±200 mV for 20–30 ms intervals and to break and reform the bilayer regularly. Possibly, bilayer imperfections assist pore insertions. If no insertion is observed and the bilayer capacitance is compatible with a properly formed lipid bilayer, more pores should be added.

Once an insertion event is observed, the first step is to balance a possible potential offset. This is done by applying zero bias potential and using the "pipette offset" to rectify the current to 0 pA. The next steps are to make sure only a single channel has inserted and to evaluate the type of nanopore. First, we check the currents at ±35 mV. In a balanced system with an accurately prepared buffer (150 mM NaCl, 15 mM Tris–HCl, pH 7.5), at a positive potential of 35 mV a stable open pore current of about 65 ± 2 pA is expected for type I ClyA-AS pores. At negative potential, the open pore current should always be lower (−60 ± 2 pA, Fig. 2A). If the former values are established, a regular type I ClyA-AS pore has inserted with its wide opening oriented to the *cis* side of the chamber (ground electrode) and its narrow entry to the *trans* side of the chamber (working electrode). A pore can also be used if it is inserted the other way around ("upside-down" pore, Fig. 2B), however, attention must be paid so that all voltages are applied oppositely. Higher currents could indicate, for example, the insertion of a different type of ClyA pore (type II is −68 ± 2 pA at −35 mV and 72 ± 2 pA at +35 mV) or multiple pores (Fig. 2C). Overall, a complete system with a ClyA pore inserted into the bilayer should have a root mean square (RMS) deviation of noise near around 2 pA using a 5 kHz bandwidth by using a Butterworth filter. This filter is always automatically applied regardless of the front-panel Bessel filter when using the I_{RMS} function of the Axopatch 200B amplifier (Molecular Devices, Axopatch 200B manual). Further, the open pore current should be stable without any current fluctuations. Whenever a fluctuating open pore current is observed, we first wait a couple of minutes. If there is no improvement, a few minutes at 0 mV or application of high potentials (±150–200 mV) for tens of milliseconds may help stabilize the nanopore. Once we establish that a low-noise single channel has inserted, we typically wait 5 min to make sure no second pore inserts. Our rationale is that pores break down in solution due to the highly diluted DDM concentration. To remove excess pores, it is also possible to perfuse the recording buffer after an insertion is observed, however, there is a risk to break the bilayer.

4. Enzymological and protein-ligand binding studies and their signals

The most important criteria when selecting a protein for our studies is that it should fit within the ClyA lumen. With type I ClyA, we find this is often the case for monomeric globular proteins of 20–45 kDa in size.

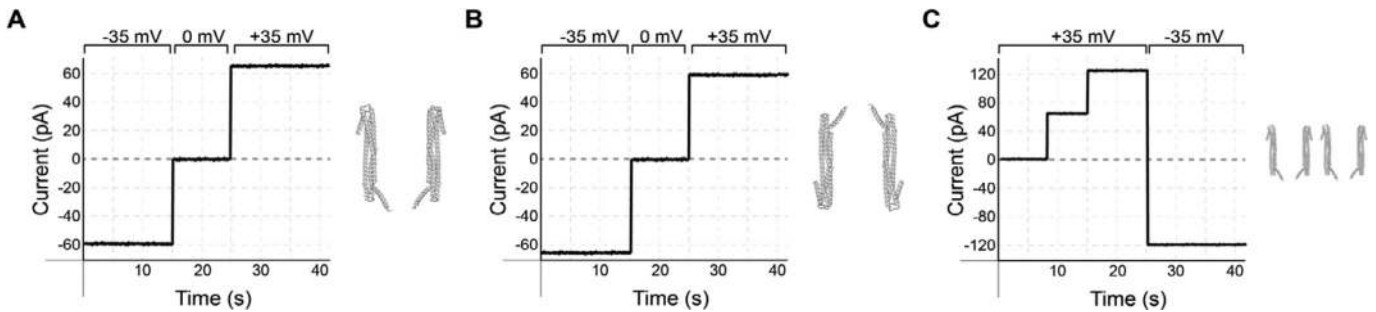

Fig. 2 Expected currents for ClyA-AS. (A) A regular ClyA-AS nanopore allows a stable current of about -60 ± 2 pA at -35 mV and 65 ± 2 pA at 35 mV to pass through in a balanced system an accurately prepared buffer of 150 mM NaCl, 15 mM Tris–HCl, pH 7.5. (B) A pore inserted in the other orientation ("upside-down") will show conversely opposite potentials. (C) Multiple pores show a larger current. The steps are shown to highlight the current contribution of a single pore. In this case two pores would have inserted in the same direction, yielding twice the current of a single pore.

Larger proteins may eclipse the pore while smaller proteins may translocate too quickly to be detected reliably. For our studies, we typically add a final protein concentration of 50–100 nM to the *cis* side of the chamber. We find this to be a good compromise between materials used and capture rates at voltages between −30 mV and −150 mV, a voltage range we commonly use for the capture of proteins. A negatively applied potential is required, because it creates an electroosmotic flow (EOF) across the nanopore from *cis* to *trans* (Willems et al., 2020), which induces the entry of the protein inside the nanopore. The latter is manifested by the decrease of the open pore current I_O to the blocked pore current I_B (Fig. 3A). In order to account for pore to pore variations, when describing current blockades, we typically use the residual current I_{RES}, which is defined as I_O/I_B (or $I_{RES\%} = I_O/I_B \times 100$). The strength of the EOF depends on the ionic concentration of the solution (Willems et al., 2020), and we typically use 150–500 mM NaCl or KCl solutions. For our recordings we typically use a sampling rate of 50–10 kHz (20–100 μs) and a Bessel filter of 10–2 kHz. The sampling rate should always be about fivefold the filtering rate.

Once a protein is inside the nanopore, the signal can be similar to the open pore current (low-noise signal) or display a variety of different current levels (Zernia, van der Heide, Galenkamp, Gouridis, & Maglia, 2020). Although the protein signal can be improved for example by introducing a charge dipole within the protein (Van Meervelt et al., 2017) or N- or C-terminal tag (Willems et al., 2019), the origin of the noise of proteins inside the nanopore is not understood. The further addition of cognate ligands to either the *cis* or *trans* chamber might induce a change in the blocked pore current (Fig. 3B). When testing a new protein, the binding of the ligands might or might not bring a change in the I_B. Thus far, 1/3 of the protein adaptors we tested showed no ligand-induced current changes (Zernia et al., 2020). Hence, when we test a ligand for the first time, we add it into the *cis* chamber at a final concentration near the bulk dissociation constant (K_d). If the K_d is unknown, we add consecutive amounts of ligands from very low to high concentrations. Another challenge is that proteins and protein in complex with a ligand can also elicit various signals. Currently we cannot predict how a signal will look for a given protein. We try to summarize possible signals and scenarios and give ideas on how to analyze data accordingly (Fig. 3). It should be noted that combinations of such types can also occur.

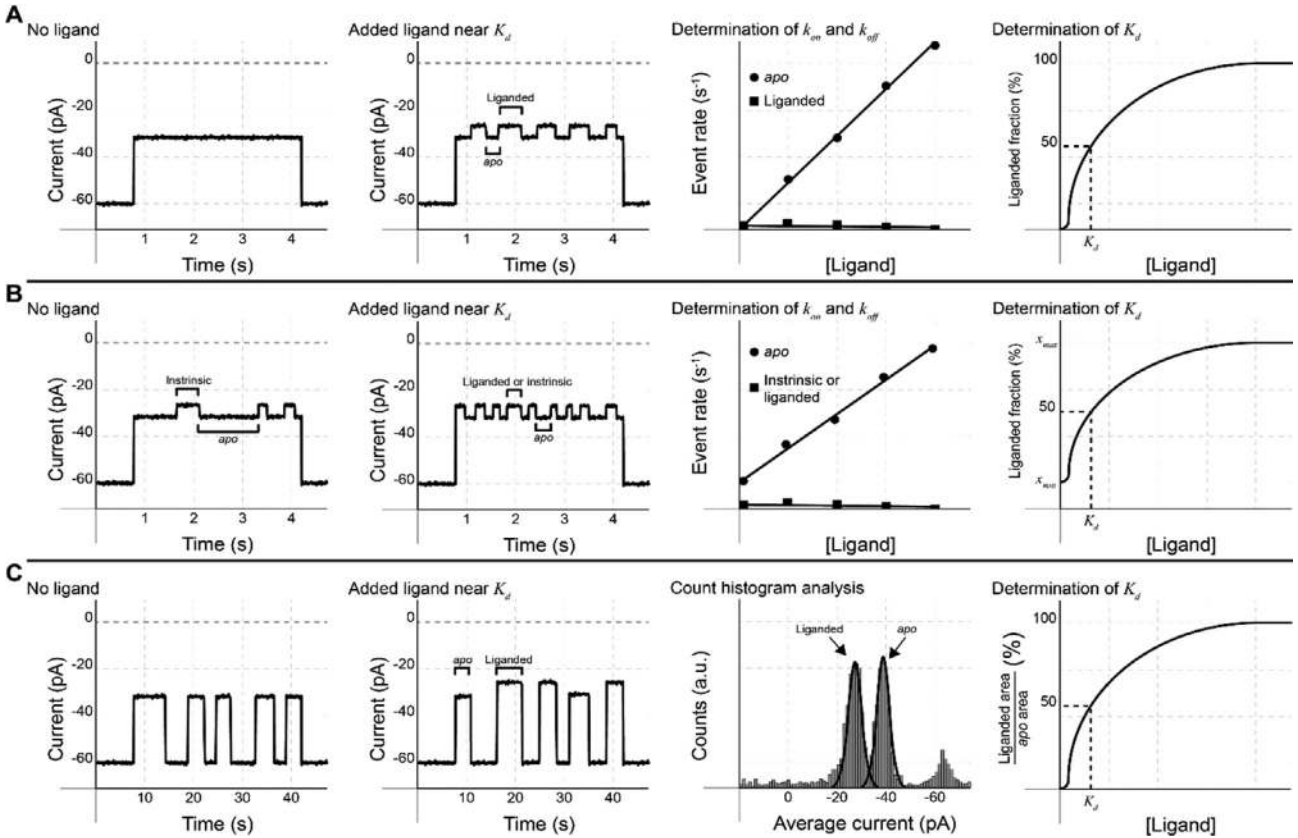

Fig. 3 See figure legend on opposite page.

4.1 Regular signals and their analysis

In the first scenario (Fig. 3A), a protein displays electrically quiet blockades with residence times of at least a few seconds. After addition of ligand, the current might increase or decrease producing an "event" within the protein blockade, reflecting the binding, and unbinding of the ligand. Under these conditions the on-rate and off-rate of the ligands can be measured (*see later*), and the concentration of the ligand in the solution can be calculated. Occasionally, we observe protein blockades of the *apo*-protein (unbound) with regular 'intrinsic' current fluctuations. We attribute this to the spontaneous closing of the protein in the absence of a ligand. The addition of the ligand then increases the frequency of current fluctuation (Fig. 3B). In a third scenario, a protein also displays electrically quiet blockades, but the addition of the ligand provokes additional and uniform protein blockades that have different residual currents (I_{RES}, Fig. 3C). If all such blockades have a different I_{RES}, it is possible that this is caused by the saturation of the ligand (i.e., all proteins are bound to the ligand and the unbinding is too fast to be detected). In this case, the concentration of the ligand should be reduced. If only a few blockades show a change in I_{RES}, then the signal can be explained by the binding of a high affinity ligand to the protein. In this case, the residence time of the protein inside the pore is shorter than the ligand off-rate and the latter cannot be detected or measured. The on-rate can often still be measured if the protein is added on the *cis* side of the nanopore and the ligand is added on the *trans* side.

On- and off-rates are calculated by measuring the time corresponding to the duration of a ligand-bound event and the time between two ligand-induced events (inter-event time). The easiest analysis is the allocation of

Fig. 3 (A) Electrically quiet protein blockades that gain an additional level upon addition of a ligand (liganded protein). By plotting the event rate per second against the ligand concentration, the k_{on} and k_{off} can be estimated. By plotting the fraction of liganded protein against the concentration of ligand, the K_d can be estimated at 50% liganded fraction. (B) Protein blockades with intrinsic events that gain frequency upon addition of a ligand (liganded protein). By plotting the event rate per second against the ligand concentration, the k_{on} and k_{off} can be estimated, however, the event rate is offset by the intrinsic events. By plotting the fraction of liganded protein against the concentration of ligand, the K_d can be estimated at 50% normalized liganded fraction, which is the liganded fraction with an offset for the intrinsic events. (C) Electrically quiet protein blockades, that when ligand is added appear to change in current. The K_d can be estimated by determining the percentage of liganded protein (relative to total protein), the K_d is the concentration in which 50% protein is liganded.

the I_{RES} of the unbound (*apo*) protein blockades and liganded protein blockades as well as the dwell times. The (semi) automatic "single-channel" search function in Clampfit 10.7 (Molecular Devices) gives the amplitudes of events, from which I_{RES} can be calculated, as well as their dwell times and other parameters. By treating all blockades separately, impurities and noise can be dealt with. Dwell times are stochastically distributed, and their values can be plotted in a cumulative or conventional histogram and fitted to one or more exponential functions, depending on the shape of the histogram. Two or more exponents should be used if the fitting is not matching the shape of the curve or two or more distributions are visible, however, it is important to check if the addition of exponents is justified. As a rule of thumb, for non-normally distributed data, the binning of the histogram with few data points should be following the Freedman-Diaconis rule (Eq. 1) (Scott, 1979; Sharma et al., 2018)

$$\Delta_b = 2\frac{(q_{75} - q_{25})}{\sqrt[3]{n}} \tag{1}$$

where Δ_b is the bin width, q_{75} is the point of the 75% quantile, q_{25} is the point of the 25% quantile and n is the number of datapoints. In practice, we fit the data several times with different binning and take the Δ_b that corresponds to one third of the fitted dwell time.

The fitting to the curve gives the dwell time parameter, tau (τ, in seconds). The off-rate (k_{off}, s^{-1}) for ligands inside the nanopore is measured from the inverse of the dwell time of the ligand-induced event and does not change whether the ligand is added to the *cis* or *trans* side. Inter-event times are related to the concentration of the ligand in bulk and to the propensity of the ligand to enter the nanopore. Plotting the inverse of the inter-event times of *apo* blockades (in events·s^{-1}) against the bulk ligand concentration should give a linear relationship whose slope is equal to the on-rate (k_{on}, $M^{-1}\,s^{-1}$) for the ligand inside the nanopore. Compared to bulk values, the nanopore-measured on-rate might be voltage dependent, especially if the ligand is charged (*see later*). Also, since the *cis* and *trans* entry of the nanopore have a different diameter, the on-rate will depend on the addition to either the *cis* or *trans* side of the nanopore. For non-charged analytes, we typically do not observe significant difference between the on-rates measured for proteins inside the nanopore (for ligands added to the *cis* compartment) compared to bulk values (Zernia et al., 2020).

The dissociation constant, K_d can be measured from the on-rate and off-rate (k_{off}/k_{on}). Alternatively, it can be calculated by plotting the percentage of signal that is in the liganded state, relative to the total signal, against the concentration of the ligand. The percentages of relative liganded population can be obtained by plotting an all-point histogram from individual protein blockades and fit normal (Gaussian) distribution functions to obtain the area under the curve for the liganded and *apo* configuration of the protein. All areas can then be added together to obtain the overall percentage of liganded and *apo* configuration.

If intrinsic closing events are observed (Fig. 3B), the obtained curve can be normalized with Eq. (2).

$$x_{norm} = \frac{x - x_{min}}{x_{max} - x_{min}} \tag{2}$$

where x_{norm} is the normalized value, x_{min} is the fraction of *apo* protein in the closed configuration measured before addition of ligand, and x_{max} is the fraction of closed protein.

The resulting apparent K_d is the point in the graph of the liganded state against the concentration, at which the liganded state amounts to 50% of the total signal. Hill function might be used to determine eventual cooperativity.

If the apparent off-rate of the ligand-induced events is longer than the residence time of the protein (Fig. 3C), we calculate the K_d by creating a histogram of the average current of a large amount of protein blockades (i.e., one protein blockade is one count). Two (or more) distributions should appear, relating to the *apo* and ligand bound state of the protein. We plot the fraction of bound protein, relative to the total number of blockades, against the concentration of ligand. The K_d is equal to the bound where 50% of the protein appears in the ligand bound state.

4.2 Complex protein signals

About one third of proteins we tested showed a non-uniform signal. Examples include blockades with multiple well-defined I_{RES} values and/or with a different level of noise (Fig. 4A). Once contaminant proteins in the solution have been ruled out, the different signals might be due to a variety of factors, including the same protein entering the nanopore with different conformations/orientation, to the intrinsic molecular noise of the protein moving inside the nanopore, or to the protein interacting with a different region within the nanopore. Upon addition of ligands, one or several levels

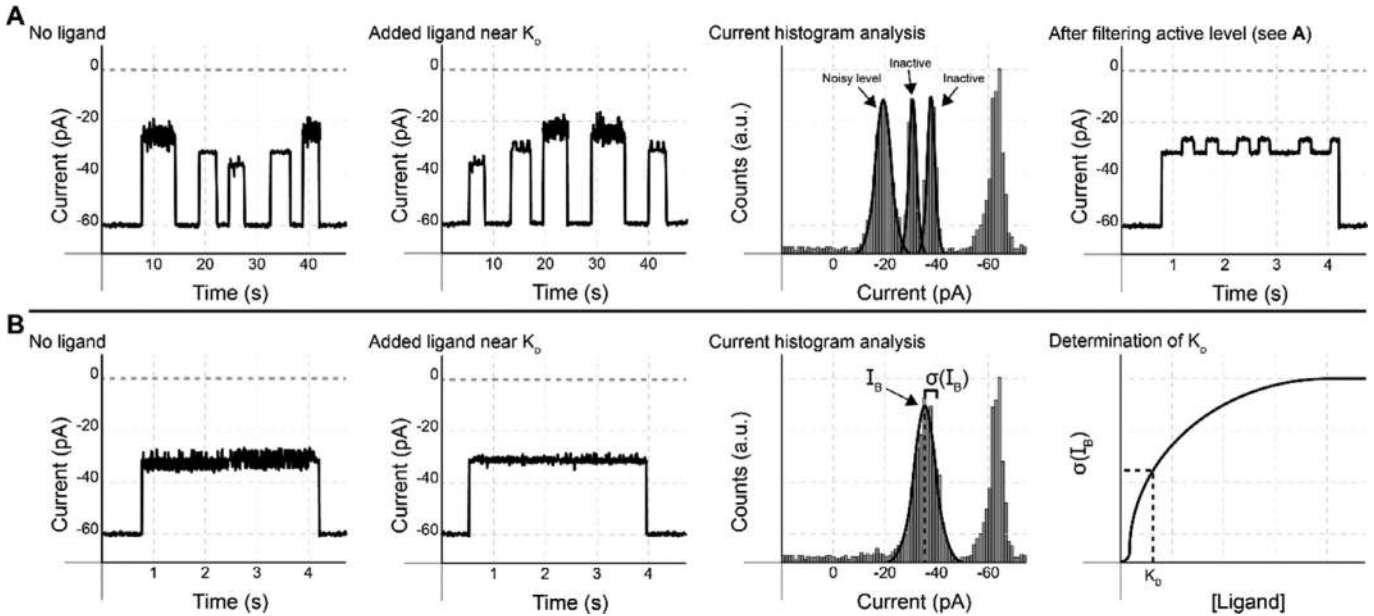

Fig. 4 (A) Protein blockades with multiple levels entering the pore. Upon addition of the ligand, a (potentially noisy) level appears in addition to the *apo* signals. The baseline current of the ligand active protein is filtered based on its current and these blockades are further analyzed. (B) Electrically noisy *apo* protein blockade with a reduced noise upon addition of ligand. The K_d is estimated by setting the standard deviation of protein blockades against the ligand concentration. The K_d is the halfway point between the *apo* protein noise and fully liganded protein noise.

may be changing (i.e. the binding of ligands induce a change in the signal), or additional blockades might be appearing, or the noise or the dwell time might change. Then, the K_d can be determined by analyzing the current blockades after ligand additions. For instance, a full point current histogram of one or more current blockades could reveal the appearance of additional peak(s) corresponding to the liganded complex (Fig. 4A). Then the relative change between the peak intensity can be plotted over the bulk concentration of ligand. The relative peak height or the area under the curve could be used. However, since a fitting a function increases error, using the peak height is often recommended. In another example we encountered, the noise might change as depicted in Fig. 4B. In this case, the standard deviation of the signal—conventionally named $\sigma(I_B)$—can be determined by fitting a normal distribution. Plotting the average $\sigma(I_B)$ against the concentration of the ligand should result in a binding curve with a minimum noise and maximum noise. The concentration of the point in between (50% increase) is the concentration of the dissociation constant (K_d).

4.3 How to improve a signal

At present we cannot predict current blockades elicited by the three-dimensional structure of a protein. However, we gained insight into how to improve a signal. When well-defined ligand-induced events are observed, optimization of the signal is obtained by varying the bias or by adjusting the ionic strength of the solution. Typically, a better signal is obtained by increasing the ionic strength or the external bias. However, ionic strengths higher than 500 mM decrease the EOF and generally reduce the residence time of a protein inside the nanopore, and/or might change the binding site of the protein within the nanopore. Similarly, high potentials might change the localization of the protein inside the nanopore, which might have an unexpected effect on the ligand-induced protein signal. Furthermore, the physical properties at which the protein of interest functions might also represents a limiting factor. Apart from the applied potential and the ionic strength, the types of salts can be varied. For example, we observe higher currents with potassium chloride instead of sodium chloride, due to the high mobility of K^+ ions. The sampling of enzymatic reactions might also require changing the pH of the solution. Within pH values of 7 to 9, we observe ClyA to still work well. Further, protein signals might also be improved by site-directed mutagenesis. For example, we tested proteins of about 20 kDa in size

displaying only short-lasting blockades. Upon introduction of a ring of tryptophan-residues (ClyA-AS-Q56W) such blockades became longer, enabling their reliable detection (Wloka et al., 2017).

It is also possible to modify the protein of interest to improve its electrical signal. For example, to increase the dwell time of a negatively charged protein inside the pore it is possible to add a positively charged tag onto the protein of interest (Biesemans, Soskine, & Maglia, 2015; Willems et al., 2019). Due to the negative voltage bias applied, molecules will experience an EOF and an electrophoretic force (EF). The EOF and the EF on the tag will be dragging the protein inside the nanopore, while the negative charge on the body of the protein will pull in the opposite direction. The positive charge tag have further electrostatic interactions with the negatively charged constriction of the nanopore that will elongate the dwell time of the protein inside the nanopore (Willems et al., 2019). We also showed that the genetic engineering of a charge dipole within a protein can allow reducing the current noise (Soskine et al., 2015; Wloka et al., 2017; Zernia et al., 2020). Most likely, the dipole allows aligning the protein to the electric field inside the nanopore and stops the protein from tumbling. These surface changes adjustments are possible with as little as changing one amino acid residue (Van Meervelt et al., 2017).

5. The effect of electrophoretic forces and nanopore confinement

To date, nanopore analysis is the only single-molecule technique for the study of native or unlabeled proteins. Other techniques require immobilization or (fluorescent) tags to study a protein of interest or introduce appendices (optical tweezers). Moreover, because a nanopore represents a relatively crowded environment, it may also offer a more natural environment than the highly diluted solutions used in other single-molecule biochemical studies performed in bulk. It was previously reported that applied voltages may unfold proteins in solid-state pores (Freedman et al., 2011; Talaga & Li, 2009). We did not find strong evidence for such an effect, and we think that the confined space in a ClyA nanopore does not have a large effect on the thermodynamic properties of a trapped protein, at least at the near-physiological conditions and moderate voltages we routinely use (−30 to −150 mV). Overall, we have found that, for uncharged ligands, the apparent dissociation constants measured inside the nanopore are similar to reported bulk values (Zernia et al., 2020). For example, the observed open

and closed conformations of a glucose binding protein matched well to NMR studies (Galenkamp, Soskine, Hermans, Wloka, & Maglia, 2018). In other examples we observed similar values for the binding of asparagine and glutamine to the respective substrate binding proteins as for ensemble single-molecule Förster resonance energy transfer measurements (Van Meervelt et al., 2017). However, when a ligand is charged, we often observe voltage dependent on-rates, which most likely reflect the altered diffusion of the ligands in the electric field inside the nanopore. In those cases, extrapolated values to zero applied potential often match bulk values (Galenkamp, Biesemans, & Maglia, 2020). Nonetheless, it is likely that the EOF and EF will have some effect on proteins inside the nanopore. For example, we found that in many cases, increasing the applied potential increases the probability of the translocation of protein across the nanopore, possibly by forcing the transient unfolding of the transmembrane alpha helices of ClyA (Soskine et al., 2012).

6. Employing proteins for quantitative measurements of small molecules in complex samples

For measuring quantitatively in highly complex samples such as blood, a key advantage of protein adaptors is that they confer their selectivity to the ClyA nanopore. We demonstrated that ligands that bind to proteins lodged inside the nanopore can be quantitatively detected in blood (Galenkamp et al., 2018). The most effective way to perform such an experiment is to first prepare a standard or calibration curve in near-physiological buffers (e.g. 150 mM NaCl, 15 mM Tris–HCl, pH 7.5). The latter is prepared by making standard additions of *known* concentrations of the analyte and the change in signal is recorded. In the simplest example, at each ligand concentration a histogram is made for each protein blockade or for a group of blockades. Then, the area under the histogram corresponding to the blocked and unblocked current signal is measured. Multiple protein blockades are usually considered for each ligand concentration. A binding isotherm is then prepared. We found that best results are obtained by plotting the ratio between the blocked and unblocked signals at different ligand concentrations. This calibration curve is then used to calculate the concentration of the ligand in an unknown sample. Although the ligand can be added to either the *cis* or *trans* chamber (but different calibration curves should be made) it is advisable to add a biological sample to the *trans* side of the nanopore when possible. The protein adaptor is always added to the *cis* side.

In this configuration, the *trans* entry of the nanopore acts as a filter for large molecules and pore clogging is normally not observed, especially if dilutions are used. Normally, the signal is not affected by the biological sample and the concentration of the ligand is extracted directly from the standard curve. For simultaneous sensing, without the need to add sequential dilutions of a sample, the tuning of an adaptor protein to the analyte's concentration range in the sample of interest is required, as demonstrated (Galenkamp et al., 2018).

References

Biesemans, A., Soskine, M., & Maglia, G. (2015). A protein rotaxane controls the translocation of proteins across a ClyA nanopore. *Nano Letters*, *15*(9), 6076–6081. https://doi.org/10.1021/acs.nanolett.5b02309.

Eifler, N., Vetsch, M., Gregorini, M., Ringler, P., Chami, M., Philippsen, A., et al. (2006). Cytotoxin ClyA from Escherichia coli assembles to a 13-meric pore independent of its redox-state. *The EMBO Journal*, *25*(11), 2652–2661. https://doi.org/10.1038/sj.emboj.7601130.

Franceschini, L., Brouns, T., Willems, K., Carlon, E., & Maglia, G. (2016). DNA translocation through nanopores at physiological ionic strengths requires precise nanoscale engineering. *ACS Nano*, *10*(9), 8394–8402. https://doi.org/10.1021/acsnano.6b03159.

Freedman, K. J., Jurgens, M., Prabhu, A., Ahn, C. W., Jemth, P., Edel, J. B., et al. (2011). Chemical, thermal, and electric field induced unfolding of single protein molecules studied using nanopores. *Analytical Chemistry*, *83*(13), 5137–5144. https://doi.org/10.1021/ac2001725.

Galenkamp, N. S., Biesemans, A., & Maglia, G. (2020). Directional conformer exchange in dihydrofolate reductase revealed by single-molecule nanopore recordings. *Nature Chemistry*, *12*(5), 481–488. https://doi.org/10.1038/s41557-020-0437-0.

Galenkamp, N. S., Soskine, M., Hermans, J., Wloka, C., & Maglia, G. (2018). Direct electrical quantification of glucose and asparagine from bodily fluids using nanopores. *Nature Communications*, *9*(1), 4085. https://doi.org/10.1038/s41467-018-06534-1.

Galenkamp, N. S., Van Meervelt, V., Mutter, N. L., van der Heide, N. J., Wloka, C., & Maglia, G. (2021). Preparation of cytolysin A (ClyA) nanopores. *Methods in Molecular Biology*, *2186*, 11–18. https://doi.org/10.1007/978-1-0716-0806-7_2.

Kwak, D. K., Kim, J. S., Lee, M. K., Ryu, K. S., & Chi, S. W. (2020). Probing the neuraminidase activity of influenza virus using a Cytolysin A protein nanopore. *Analytical Chemistry*, *92*(21), 14303–14308. https://doi.org/10.1021/acs.analchem.0c03399.

Li, X., Lee, K. H., Shorkey, S., Chen, J., & Chen, M. (2020). Different anomeric sugar bound states of maltose binding protein resolved by a cytolysin A nanopore tweezer. *ACS Nano*, *14*(2), 1727–1737. https://doi.org/10.1021/acsnano.9b07385.

Ludwig, A., Bauer, S., Benz, R., Bergmann, B., & Goebel, W. (1999). Analysis of the SlyA-controlled expression, subcellular localization and pore-forming activity of a 34 kDa haemolysin (ClyA) from Escherichia coli K-12. *Molecular Microbiology*, *31*(2), 557–567. https://doi.org/10.1046/j.1365-2958.1999.01196.x.

Maglia, G., Heron, A. J., Stoddart, D., Japrung, D., & Bayley, H. (2010). Analysis of single nucleic acid molecules with protein nanopores. *Methods in Enzymology*, *475*, 591–623. https://doi.org/10.1016/S0076-6879(10)75022-9.

Montal, M., & Mueller, P. (1972). Formation of bimolecular membranes from lipid monolayers and a study of their electrical properties. *Proceedings of the National Academy of Sciences of the United States of America*, *69*(12), 3561–3566. https://doi.org/10.1073/pnas.69.12.3561.

Mueller, M., Grauschopf, U., Maier, T., Glockshuber, R., & Ban, N. (2009). The structure of a cytolytic alpha-helical toxin pore reveals its assembly mechanism. *Nature*, *459*(7247), 726–730. https://doi.org/10.1038/nature08026.

Nomidis, S. K., Hooyberghs, J., Maglia, G., & Carlon, E. (2018). DNA capture into the ClyA nanopore: Diffusion-limited versus reaction-limited processes. *Journal of Physics. Condensed Matter*, *30*(30), 304001. https://doi.org/10.1088/1361-648X/aacc01.

Nymeyer, H., & Zhou, H. X. (2008). A method to determine dielectric constants in non-homogeneous systems: Application to biological membranes. *Biophysical Journal*, *94*(4), 1185–1193. https://doi.org/10.1529/biophysj.107.117770.

Peng, W., de Souza Santos, M., Li, Y., Tomchick, D. R., & Orth, K. (2019). High-resolution cryo-EM structures of the E. coli hemolysin ClyA oligomers. *PLoS One*, *14*(5), e0213423.. https://doi.org/10.1371/journal.pone.0213423

Scott, D. W. (1979). On optimal and data-based histograms. *Biometrika*, *66*(3), 605–610. https://doi.org/10.1093/biomet/66.3.605.

Sharma, S. K., Kumar, S., & Karmeshu. (2018). Suppression of multimodality in inter-spike interval distribution: Role of external damped oscillatory input. *IEEE Transactions on Nanobioscience*, *17*(3), 329–341. https://doi.org/10.1109/TNB.2018.2845454.

Soskine, M., Biesemans, A., De Maeyer, M., & Maglia, G. (2013). Tuning the size and properties of ClyA nanopores assisted by directed evolution. *Journal of the American Chemical Society*, *135*(36), 13456–13463. https://doi.org/10.1021/ja4053398.

Soskine, M., Biesemans, A., & Maglia, G. (2015). Single-molecule analyte recognition with ClyA nanopores equipped with internal protein adaptors. *Journal of the American Chemical Society*, *137*(17), 5793–5797. https://doi.org/10.1021/jacs.5b01520.

Soskine, M., Biesemans, A., Moeyaert, B., Cheley, S., Bayley, H., & Maglia, G. (2012). An engineered ClyA nanopore detects folded target proteins by selective external association and pore entry. *Nano Letters*, *12*(9), 4895–4900. https://doi.org/10.1021/nl3024438.

Talaga, D. S., & Li, J. (2009). Single-molecule protein unfolding in solid state nanopores. *Journal of the American Chemical Society*, *131*(26), 9287–9297. https://doi.org/10.1021/ja901088b.

Van Meervelt, V., Soskine, M., Singh, S., Schuurman-Wolters, G. K., Wijma, H. J., Poolman, B., et al. (2017). Real-time conformational changes and controlled orientation of native proteins inside a protein nanoreactor. *Journal of the American Chemical Society*, *139*(51), 18640–18646. https://doi.org/10.1021/jacs.7b10106.

von Rhein, C., Bauer, S., Lopez Sanjurjo, E. J., Benz, R., Goebel, W., & Ludwig, A. (2009). ClyA cytolysin from Salmonella: Distribution within the genus, regulation of expression by SlyA, and pore-forming characteristics. *International Journal of Medical Microbiology*, *299*(1), 21–35. https://doi.org/10.1016/j.ijmm.2008.06.004.

Willems, K., Ruic, D., Biesemans, A., Galenkamp, N. S., Van Dorpe, P., & Maglia, G. (2019). Engineering and modeling the electrophoretic trapping of a single protein inside a nanopore. *ACS Nano*, *13*(9), 9980–9992. https://doi.org/10.1021/acsnano.8b09137.

Willems, K., Ruic, D., Lucas, F. L. R., Barman, U., Verellen, N., Hofkens, J., et al. (2020). Accurate modeling of a biological nanopore with an extended continuum framework. *Nanoscale*, *12*(32), 16775–16795. https://doi.org/10.1039/d0nr03114c.

Wloka, C., Van Meervelt, V., van Gelder, D., Danda, N., Jager, N., Williams, C. P., et al. (2017). Label-free and real-time detection of protein ubiquitination with a biological nanopore. *ACS Nano*, *11*(5), 4387–4394. https://doi.org/10.1021/acsnano.6b07760.

Zernia, S., van der Heide, N. J., Galenkamp, N. S., Gouridis, G., & Maglia, G. (2020). Current blockades of proteins inside nanopores for real-time metabolome analysis. *ACS Nano*, *14*(2), 2296–2307. https://doi.org/10.1021/acsnano.9b09434.